Polymer Chemistry

PAPER

View Article Online
View Journal | View Issue

Cite this: *Polym. Chem.*, 2019, **10**, 386

"Carbolong" polymers with near infrared triggered, spatially resolved and rapid self-healing properties†

Huan Zhang, ‡[a] Haibo Zhao,‡[a,b] Kaiyue Zhuo,[a,b] Yuhui Hua,[a,b] Jiangxi Chen, [c] Xumin He,*[a,b] Wengui Weng *[a] and Haiping Xia *[a,b]

Received 17th October 2018,
Accepted 30th November 2018

DOI: 10.1039/c8py01482e

rsc.li/polymers

Metallopolymers combine the functionality of metal centres with the processabilities of polymers, leading to rapidly expanding interest in the design and development of novel functional materials and devices. Carbolong complexes are a brand-new family of Möbius metalla-aromatics among which specific structures exhibit excellent photothermal properties under near infrared (NIR) light. Here, NIR photothermally healable carbolong polyurethanes (CLPUs) carrying covalently embedded 12C-carbolong motifs in the backbone are reported for the first time. CLPUs with a very low content of 12C-carbolong (down to 0.10 wt%) exhibit fast (<1 min), spatially resolved, and repeatable (>5 cycles) healing whose efficiency can be tuned by the content of the carbolong complex and NIR power. The healing mechanism is ascribed to the accelerated dissociation of physical interactions, melting of polymer crystallites and chain diffusion induced by the NIR photothermal effect of carbolong embedded in the CLPUs. The fruitful chemistry and the unique photothermal properties of carbolong complexes make them versatile for the design of light-controlled and light-powered self-healing materials.

1. Introduction

Synthetic polymers that contain metal centres as building blocks, *i.e.*, metallopolymers, have sparked a great deal of interest in the past decade because of their unique properties.[1] The presence of metal elements in a polymer chain provides a versatile platform for combining the chemical, electronic, magnetic, optical, redox, catalytic, and mechanical properties of metal centres with the synthetic efficiencies and ready processabilities of organic polymers. So far, a variety of metal centres have been harnessed and incorporated into polymer backbones, including but not limited to lanthanides and main- and transition-group metals. The interactions between the metal ions and the ligands can be tailored to vary continuously from strong and static binding (covalent) to weak and reversible coordination interactions (non-covalent).[2] Moreover, the location of the metal centres in the polymer chain (the main chain[3] or the side chain[4,5]) and the chain topology (linear, branched or dendritic[6]) offer metallopolymers great flexibilities in the structure and architecture design. Such structural and dynamic diversity have secured a prominent role of metallopolymers in a myriad of applications as diverse as photovoltaics,[7] data storage,[8] catalysis,[9] and stimuli-responsive[10,11] and self-healing materials.[3,12–17]

Among various metal–ligand complexes, polymers carrying "carbolong" complexes are rarely explored.[18–20] Carbolong complexes are a brand-new family of Möbius metalla-aromatics developed by the Xia group, in which the transition metal chelates with highly conjugated carbon ligands.[21–25] Carbolong complexes are particularly useful to construct functional polymeric materials because of their (a) fruitful chemistry to be covalently incorporated into polymers,[18–20] enabling versatile polymer design, and (b) excellent optical,[26] single-molecular conductive,[27] photoacoustic,[28] and particularly photothermal properties, depending on their specific structures.[18–20,22,29]

Self-healing materials are one kind of intelligent material that can recover functions and mechanical properties after

[a]*Department of Chemistry, College of Chemistry and Chemical Engineering, Xiamen University, Xiamen 361005, China. E-mail: wgweng@xmu.edu.cn*
[b]*State Key Laboratory of Physical Chemistry of Solid Surfaces and Collaborative Innovation Centre of Chemistry for Energy Materials (iChEM), Xiamen University, Xiamen 361005, China. E-mail: hejin@xmu.edu.cn, hpxia@xmu.edu.cn*
[c]*Department of Materials Science and Engineering, College of Materials, Xiamen University, Xiamen 361005, China*

†Electronic supplementary information (ESI) available: ^{1}H NMR, ^{13}C NMR, ^{31}P NMR, two-dimensional ^{1}H–^{13}C HSQC and HMBC spectra, X-ray crystallography, DEPT-135, ESI-MS, and UV spectra of carbolong complexes, GPC traces, XRD, SAXS and stress–strain curves of CLPU films, thermographic images, optical images, stress–strain curves, healing efficiency for self-healing of CLPU films. CCDC 1868666. For ESI and crystallographic data in CIF or other electronic format see DOI: 10.1039/c8py01482e

‡These authors contributed equally to this work.

damage. Among various ways to achieve self-healing, light initiated self-healing processes provide a convenient way to remotely control the mending of materials in a spatiotemporal manner *in situ*. The underlying healing mechanisms may involve photo-crosslinking reactions, photoinduced metathesis,[30] and photothermal effects, *i.e.*, the conversion of photons into heat *via* non-radioactive relaxation mechanisms.[31–34] For instance, Rowan and co-workers pioneered a metallo-supramolecular polymer carrying a metal–ligand complex that exhibits fast and efficient healing upon UV irradiation.[3] For those self-healing dynamic polymers, the heat generated by light not only promotes local chain diffusion across the interface of wounded regions but also accelerates the dissociation of dynamic bonds like a metal–ligand complex,[3] hydrogen bonding,[35] and Diels–Alder adduct.[36] Near infrared (NIR) light irradiation is advantageous over UV light due its low photochemical effect and deep sample penetration. So far, a variety of photothermal conversion reagents has been reported for self-healing applications, such as gold nanoparticles,[32,37,38] carbon nanotubes[36] and graphenes,[35] and conjugated polymers.[39] Although these materials are efficient and promising to prepare self-healing polymers, they form heterogeneous systems and usually have poor interfacial interactions with a polymer matrix.[40] On the basis of the fruitful chemistry and excellent NIR photothermal properties of carbolong, we envisage that polymers covalently carrying carbolong complexes may achieve spatially resolved, repeated and fast healing of materials in a remote way by light. In this regard, Xia and co-workers have successfully synthesized copolymers,[18] tadpole-like amphiphilic polymers,[19] and cylindrical polymers with carbolong complexes on the side groups or chain ends in preliminary attempts.[20] All three metallopolymers exhibited excellent photothermal properties under NIR light irradiation.

Herein, for the first time, we report on the development of NIR photothermally healable carbolong polyurethanes (CLPUs) by covalently incorporating carbolong complexes into the backbones of linear polyurethanes (Fig. 1). CLPUs with very low contents of carbolong exhibited fast and highly efficient photothermal responses under NIR irradiation and the photothermal effect could be readily modulated by the content of carbolong complexes and the light intensity. The strong photothermal effect allowed not only NIR-triggered, fast (<30 s) and repeatable (>5 cycles) healing of CLPUs, but also localized spatiotemporal control of the healing process. We hope that our demonstration will pave the way for the applications of carbolong complexes in a variety of versatile self-healable polymeric materials.

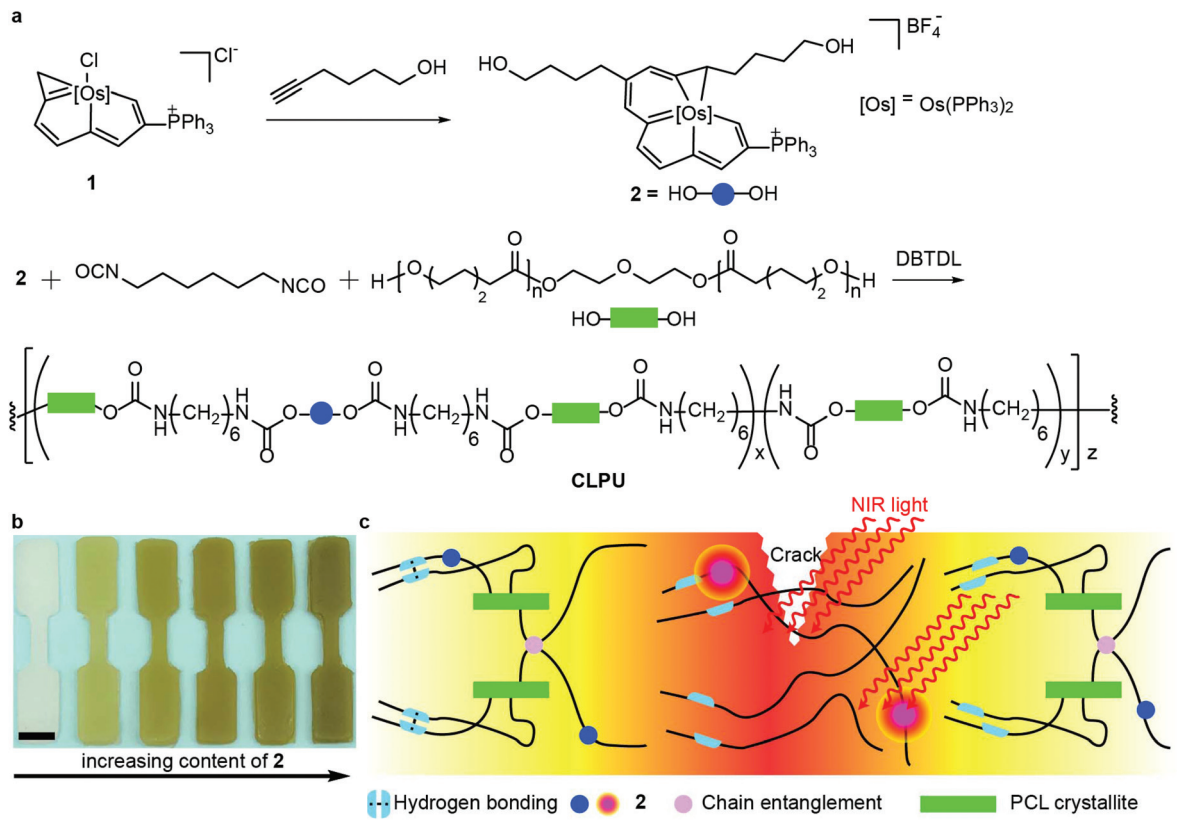

Fig. 1 (a) Synthesis of dihydroxyl 12C-carbolong complex **2** containing polymerisable groups and the corresponding carbolong polyurethanes. (b) CLPU specimens of **CLPU0**, **CLPU7**, **CLPU10**, **CLPU15**, **CLPU20**, and **CLPU30** (from left to right). The scale bar is 0.5 cm. (c) Schematic illustration of the NIR triggered healing process.

2. Results and discussion

2.1. Synthesis of dihydroxyl 12C-carbolong complex 2

A 12C-carbolong complex **1** was first synthesized and further derived with hex-5-yn-1-ol to give a dihydroxyl carbolong complex **2** in 90% yield according to Xia's reported route (Fig. 1a).[22] The chemical structure of **2** was confirmed by NMR spectroscopy, X-ray crystallography, and liquid chromatography–mass spectrometry (Fig. S1–S8 and Table S1†). To prepare carbolong polyurethanes, **2** was polymerized with 1,6-hexyldiisocyanate and poly(ε-caprolactone) (PCL, number averaged molecular weight M_n = 2 kDa). PCL would impart good mechanical and potential shape memory properties to CLPUs, and its melting and recrystallization are of importance to self-healing. The molecular weight of CLPUs was determined by gel permeation chromatography (GPC, Fig. S9–S14†) and is listed in Table S2.† The M_n of all samples is in the range of 95–150 kDa with a polydispersity of 1.30–1.78. The content of **2** in the CLPUs was determined by UV-vis against a standard curve (Fig. S15†) and ranged from 0 to 0.30 wt% (Table S2†). Samples are denoted as **CLPU*X*** where *X*/100% is the weight percent of complex **2**. For example, **CLPU20** denotes that the content of **2** in polyurethane is 0.20 wt%. Thin films (*ca.* 0.7 mm thick) of CLPUs were prepared by solution drop-casting. The as-prepared films were flexible and mechanically freestanding at room temperature. As shown in Fig. 1b, the colour of the films gradually changes from white to dark yellow by increasing the content of **2**.

2.2. Microstructure, thermal and mechanical properties of CLPU films

We first characterized the microstructure, thermal, and mechanical properties of these carbolong polyurethane films. Fig. 2a depicts the X-ray diffraction (XRD) profiles of **2**, **CLPU0**, and **CLPU20**. The XRD profile of 12C-carbolong complex **2** is featureless in the studied 2θ range, whereas two sharp peaks appear at 2θ = 21.4° and 23.7° for all CLPU films (Fig. 2a and Fig. S16–S17†), which, respectively, represent the (110) and (200) crystal planes of the PCL crystallite.[41,42] This result indicates that **2** did not disturb the crystallization of PCL segments in the CLPUs.

To explore the long-ranged morphology, we performed small angle X-ray scattering (SAXS) on CLPU films (Fig. 2b). A shoulder peak can be recognized at around q = 0.35 nm^{-1} for **CLPU0**, which comes from the interference of scattering objects within the samples. To estimate the precise peak position, we applied Lorentz correction to the scattering data (Fig. S18†)[43] and the peak position was determined to be q^* =

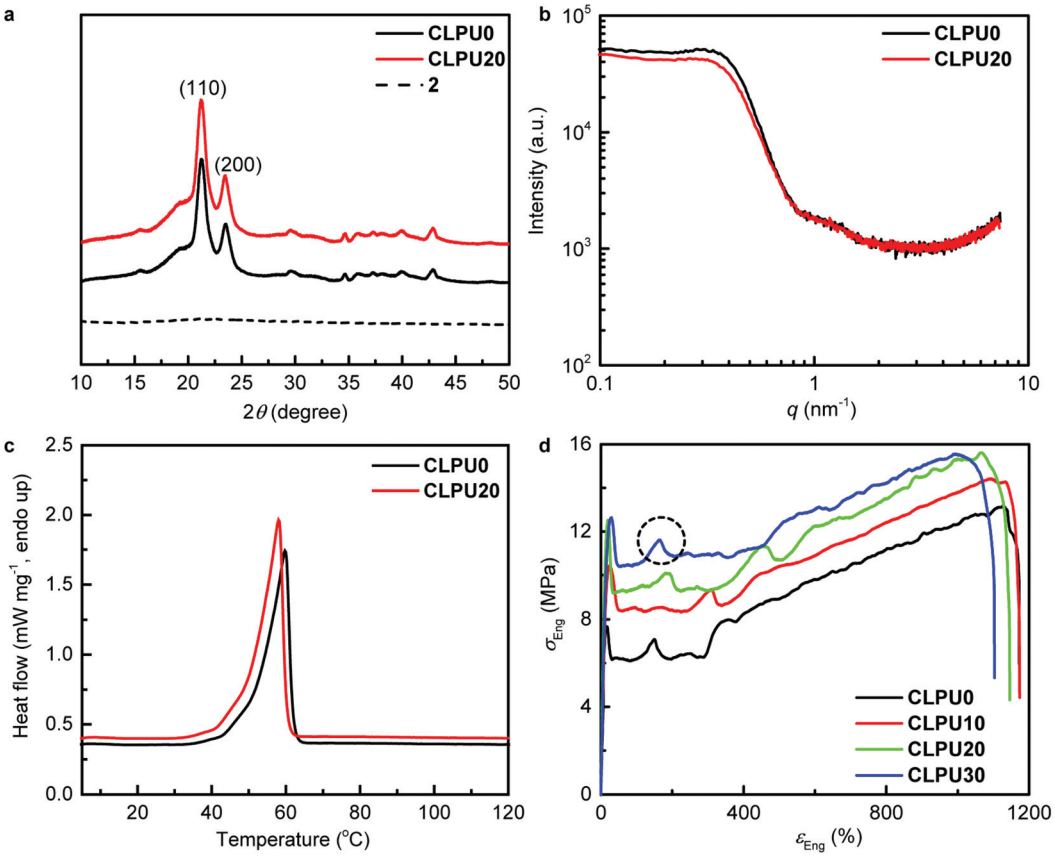

Fig. 2 (a) XRD, (b) SAXS, and (c) DSC of **CLPU0** and **CLPU20**. (d) Stress–strain curves of CLPU films with varying contents of **2** as indicated in the legend. The dashed circle indicates the sawtooth feature during plastic deformation.

0.40 nm^{-1}, which corresponds to a characteristic length $l^* = 15.7$ nm ($2\pi/q^*$). We assigned this length to the inter-lamellar spacing of the PCL crystallite according to literature studies.[41,42] Nevertheless, **CLPUs** show similar SAXS profiles to the control **CLPU0** in terms of both the scattering intensity and the peak position (Fig. S18–S19†), indicating that the presence of **2** did not result in a new long-ranged morphology.

Fig. 2c shows the differential scanning calorimetry (DSC) curves of **CLPU0** and **CLPU20**. The pure polyurethane film has an endothermic peak at 59 °C and this peak slightly shifts to a lower temperature (58 °C) for **CLPU20**. In line with the DSC results, the two diffraction peaks of the PCL crystallite disappeared at 60 °C for both **CLPU0** and **CLPU20** (Fig. S17†). Therefore, we ascribe the endothermic peak in Fig. 2c to the melting of the PCL crystallite.[37]

The shape of the stress–strain curves of all CLPUs is typical of semi-crystalline polymers (Fig. 2d and Fig. S20†). After passing the elastic region, necking initiates and continues to propagate along the entire length of the gauge section. The final ascent of the stress–strain curves displays sawtooth fluctuations (dashed circle) which can be attributed to the cold drawing of the materials from the gripped region of the specimen.[44]

Mechanical properties of CLPUs such as Young's modulus, yield strength and ultimate strength and more are listed in Table S3.† The introduction of carbolong complex **2** shows no systematical or consistent effects on these parameters. The variation of the mechanical properties (*e.g.*, Young's modulus and yield strength) is more likely due to the variation of the molecular weight and the polydispersity of these carbolong polyurethanes.

Collectively, the above results suggest that the incorporation of carbolong complex **2** into polyurethane has no obvious impacts on the microstructure, thermal, and mechanical properties of the polymer matrix. This is of particular importance for practical applications of the carbolong polyurethanes where the processing conditions of the products can be retained to the greatest extent.

2.3. Photothermal properties

We next investigated the photothermal properties of the CLPUs. UV-vis spectra of CLPUs in dimethylformamide (DMF) show excellent absorption across a wide wavelength region (Fig. 3a). We chose NIR irradiation for photothermal tests because of its low energy and deep sample penetrability. Rectangular samples were irradiated with an intensity-modulated NIR solid-state diode laser (λ = 808 nm, diameter of the beam spot: 1.1 cm). The increase of the surface temperature at the laser spot was recorded as a function of irradiation time by using a thermal infrared camera. Typical thermographic images of **CLPU20** under 0.5 W cm^{-2} NIR irradiation are depicted in Fig. 3b and Fig. S21.† When irradiated, the polymer did not show any visible fluorescence emission, and the photons absorbed by the polymer were converted to heat. As shown in Fig. 3c, the surface temperature of **CLPU20** at the beam centre rapidly increases to more than 55 °C within 1 min and reaches a steady-state because of the quasi-equilibrium between light-to-heat conversion of **2** and the thermal dissipation of the polymer matrix to the environment. CLPUs with different contents of **2** all show similar photothermal behaviour. In stark contrast, the control **CLPU0** shows little temperature increase (4 °C) under the same conditions. To the best of our knowledge, such rapid and efficient photothermal responses of polymers having chemically incorporated photothermal agents are still rare. We then explored the effects of the content of carbolong complex **2** and the power density of the laser on the photothermal performance of CLPU films (Fig. 3c and d). At a fixed power density of 0.50 W cm^{-2}, the temperature increase at the steady-state, ΔT_{ss}, clearly depends on the content of **2**. For example, ΔT_{ss} increases from 30 to 70 °C as the content of **2** changes from 0.07 to 0.30 wt%, respectively. On the other hand, ΔT_{ss} is also dependent on the laser power for a given content of **2**. For quantitative analysis, the temperature increase, ΔT, was fitted to a phenomenological exponential function $\Delta T = \Delta T_{ss}\,(1 - e^{-kt})$ where k denotes the apparent rate constant of the photothermal conversion process and t is the irradiation time of the laser.[45] The effects of the content of **2** and the power density of the laser on ΔT_{ss} and k are shown in Fig. 3e and f. ΔT_{ss} as a function of the content of **2** displays two different linear regimes with a break temperature of 55 °C. After passing this point, increasing the content of **2** causes decreased heating efficiency (the slope of the two dashed lines). Interestingly, similar behaviour with a break around 63 °C was observed when ΔT_{ss} is plotted as a function of laser power. In other words, increasing the laser power above this break point is less efficient in heating the polymer. So far, the detailed molecular origin of this behaviour has been elusive, but it might be related to the melting of the PCL crystallites as the crossover temperatures shown in Fig. 3e and f are both higher than the melting temperature of the PCL crystallite (Fig. 2c). In general, the specific heat capacity of the crystalline phase is usually smaller than that of the amorphous phase for the same polymer, and therefore the heat accumulation is more efficient when the crystalline phase is present. Moreover, the apparent rate constant of the photothermal conversion, k, has an average value of 1.17 ± 0.13 min^{-1} (except the control **CLPU0**) and is insensitive to the content of **2** (0.07–0.30 wt%) or the laser power (0.33–0.74 W cm^{-2}), suggesting that k captures the inherent photothermal kinetics of **2**.

In consideration of the importance for applications, the photothermal stability of **2** was investigated by subjecting the **CLPU20** film to 6 ON/OFF light irradiation cycles at a power of 0.5 W cm^{-2} (Fig. 3g and Fig. S22†). The temperatures at the peaks and valleys remain almost unchanged (±0.5 °C), which attests the photothermal stability of CLPU films in long-term service.

2.4. Self-healing properties

Having understood the photothermal properties of the carbolong polyurethanes, we then directed our efforts to explore their self-healing properties. In the first demonstration, we focused on the healing of microcracks. In this regard, a 0.5 mm deep cut was made on the surface of the 0.7 mm thick

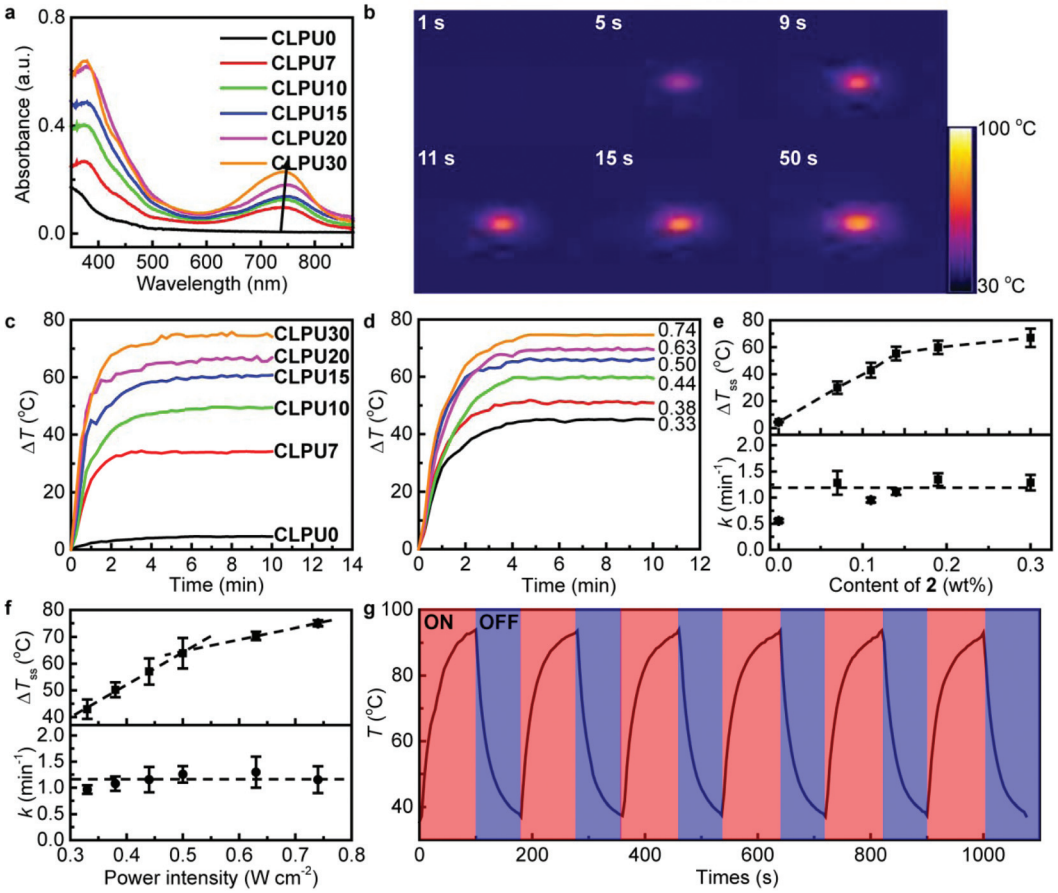

Fig. 3 Optical and photothermal properties of CLPU films. (a) UV-vis spectroscopy. The arrow indicates the increase of the content of **2**. (b) Typical thermographic images of **CLPU20** under NIR light (λ = 808 nm, 0.5 W cm^{-2}) at given times. All the thermographic images are in the same scale range. (c and d) The increase of temperature, ΔT, as a function of irradiation time with (c) varying contents of **2** (laser power density 0.5 W cm^{-2}) and (d) varying laser power densities (W cm^{-2}, indicated in numbers) for **CLPU20**. (e and f) The temperature increase at the steady state, ΔT_{ss}, and the apparent rate constant of the photothermal conversion, k, as a function of (e) the content of **2** and (f) the laser power density. Error bars are the standard deviation from three independent measurements. (g) Temperature variation of **CLPU20** under ON/OFF NIR irradiation for 6 cycles.

films for all samples. The cut was then irradiated with NIR light (λ = 808 nm) and a photograph of the crack was taken by using an optical microscope at a given time. For most of the samples, the crack closed within 10 min after irradiation and the more carbolong complex **2** was loaded, the faster the crack closed (Fig. 4 and Fig. S23†). For example, a film of **CLPU20** showed complete healing within 15 s compared to that of 50 s for **CLPU10** and more than 540 s for **CLPU7**. The fast and efficient healing can be more clearly observed from the video (ESI†). On the other hand, the control sample **CLPU0** showed no healing even after 10 minutes of NIR irradiation, suggestive of the key role of carbolong complex **2** in this NIR-triggered healing process. To the best our knowledge, examples of metallopolymers that show photothermal healing as a consequence of the NIR photothermal effect of the organometallic complex are very limited.

We next turned to verify the spatially resolved self-healing of CLPU films. Particularly, we cut a long crack (>3 cm, 0.5 mm deep) across a **CLPU20** film and irradiated the centre of the crack with NIR light for 15 s (diameter of the spot was 1.1 cm, Fig. 5a). Fig. 5b shows the photographs of the crack at different distances from the spot centre before and after irradiation. As expected, the crack within the beam spot was completely healed, whereas that just outside the spot (±0.7 cm away from the spot centre) remained unchanged. We attribute this result to the temperature gradient of the sample around the light spot (Fig. 3b), as only the irradiated area could convert light into heat and the surface temperature is the highest at the spot centre and then drastically decreases to ambient temperature with increasing distance from the spot centre. For those areas far from the laser spot, the temperature is not sufficient to initiate self-healing.

Having demonstrated the light-triggered self-healing of carbolong polyurethanes, we turned to evaluate the recovery of mechanical properties. As shown in Fig. 6a, dog-bone shaped specimens were punched from a **CLPU20** film. For each specimen, we cut a notch at the gauge section (0.5 mm wide, the width of the gauge section is 2.0 mm). The two faces of the notch were kept in contact and then irradiated with NIR light for 15 s. For some specimens, we repeated the notching–

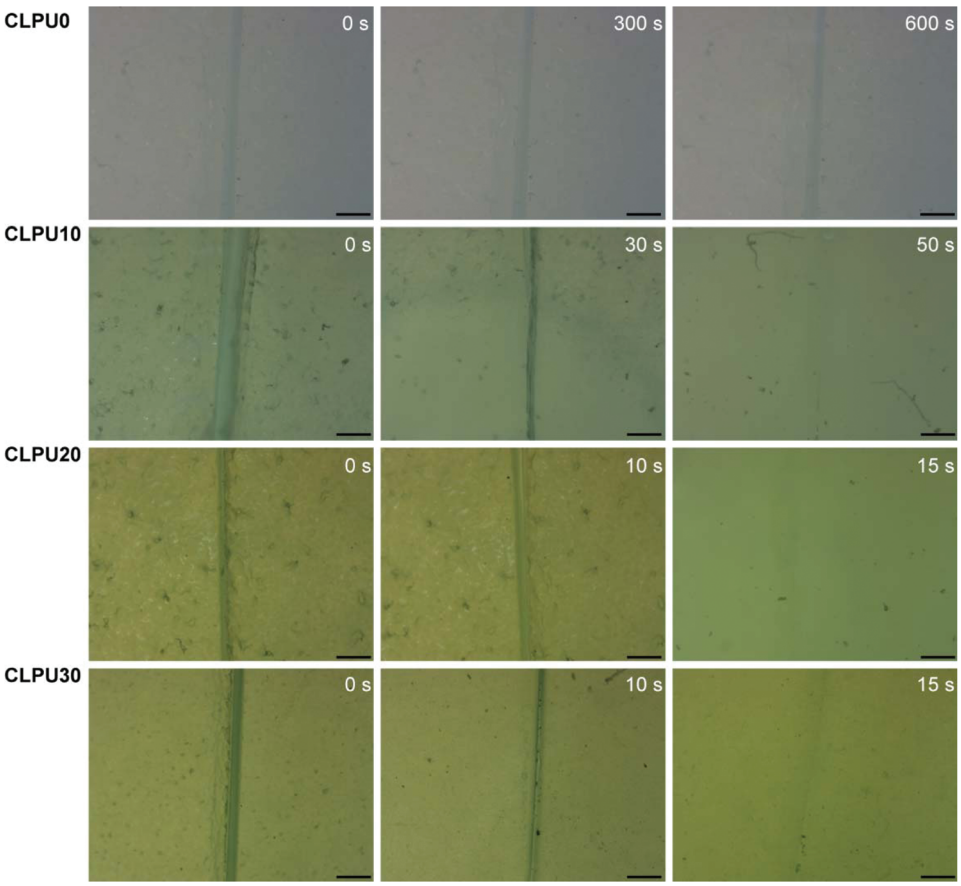

Fig. 4 Optical images of the healing process for **CLPU0**, **CLPU10**, **CLPU20**, and **CLPU30** after NIR irradiation (λ = 808 nm, 0.5 W cm^{-2}). The numbers indicate the irradiation time. The scale bar is 200 μm.

healing cycle several times at the same position and they were denoted as **CLPU20-*X*** where *X* represents the notching–healing cycles. We define the healing efficiency η as the restoration of toughness (the area under the stress–strain curve), that is, the ratio of toughness of the healed specimen to that of the pristine one (no notch). Typical stress–strain curves of pristine, notched, and healed specimens are shown in Fig. 6b. Unlike the pristine sample, the notched specimen showed no necking after passing the yield point and failed at much smaller strain (<200%) compared with that of the pristine specimen (1100%) because of the fast propagation of the notch. In stark contrast, necking behaviour appeared again in the healed specimen **CLPU20-1** and the specimen almost regained the mechanical properties. Moreover, the specimen after repeated notching–healing cycles like **CLPU20-3** and **CLPU20-5** showed a similar mechanical performance to **CLPU20-1**. Quantitatively, η of all healed **CLPU20** specimens is above 85% (Fig. 6c). We conducted similar experiments on other CLPU films. To achieve a similar value of η, longer irradiation time was required for samples with a lower content of **2** (Fig. S24–25 and Table S4†). In stark contrast, the control **CLPU0** showed no healing at all. The above results are consistent with the optical observation shown in Fig. 4.

Based on the above results, we propose here a simplified healing mechanism (Fig. 1d). When the crack is irradiated under NIR irradiation, the chemically incorporated carbolong complex **2** within the beam spot efficiently converts light into thermal energy. The cumulated heat leads to an abrupt increase in the local temperature which is sufficient to dissociate physical interactions (*i.e.* hydrogen bonding) and accelerates the chain diffusion (by melting PCL crystallites and releasing constraints due to chain entanglement, *etc.*) across the wounded interfaces, leading to the closure of the crack. Once the NIR irradiation is removed, the local temperature decreases to an environmental value (room temperature). As a consequence, physical interactions reform, PCL segments recrystallize, constraints rebuild and chain dynamics slows down, and as a result, the sample regains its mechanical properties.

3. Experimental

3.1. Synthesis of dihydroxyl 12C-carbolong complex 2

The sources of all reagents, chemicals, materials, and solvents involved in the synthesis and the functionalization of carbo-

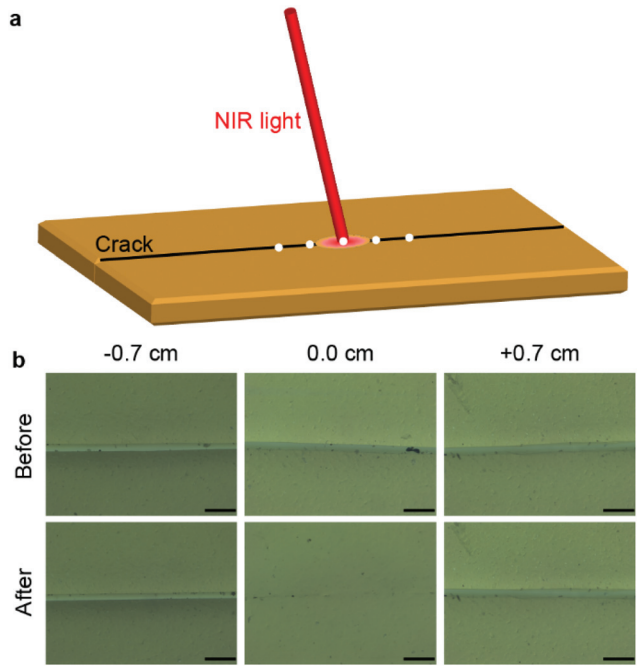

Fig. 5 Spatially resolved healing of a **CLPU20** film. (a) Schematic drawing of the test. White dots represent the sampling position along the crack. (b) Optical images of the crack at a given position before and after NIR irradiation for 15 s. The numbers denote the distance from the center of the laser spot. The diameter of the laser spot is 1.1 cm and the scale bar is 100 μm.

long complex **1** are listed and described in the ESI.† Briefly, **1** was synthesized according to the literature.[22] For functionalization, hex-5-yn-1-ol (496 μL, 4.5 mmol, 5 eq.) was injected into a mixture of **1** (1000 mg, 0.9 mmol, 1 eq.) and silver tetrafluoroborate (526 mg, 2.7 mmol, 3 eq.) in dichloromethane (20 mL). The reaction mixture was stirred at 30 °C for 5 h to yield a green solution, and then the solid suspension was removed by filtration. The filtrate was reduced under vacuum to approximately 2 mL, and then purified by column chromatography (neutral alumina, eluent: dichloromethane/methanol = 5 : 1) to give a green solution. The green solid of complex **2** (1100 mg, 90%) was collected after the solvent was evaporated to dryness under vacuum and the resulting residue was washed with diethyl ether and then dried under vacuum. Detailed structural and spectroscopic characterization of **2** is shown in Fig. S1–S8 and Table S1.†

3.2. Synthesis of CLPUs

For a typical polyurethane reaction, **2**, 1,6-diisocyanatohexane (911 μL, 5.67 mmol), dry PCL (M_n = 2000 g mol^{-1}, 10 g, 5 mmol), and dibutyltin dilaurate (DBTDL, 5 μL) were mixed with 50 mL of DMF in a 100 mL flask. N_2 was pumped into the flask three times to get rid of the oxygen. The mixture was reacted at 50 °C for 12 h to yield polyurethane. The polymer was then precipitated twice by methanol to remove oligomers and unreacted reagents. We systematically varied the initial content of **2** (0–0.5 wt%) in the reaction mixture and the accurate value in the final CLPUs was determined by UV-vis spectroscopy against a standard curve.

3.3. Film preparation

1.1 g of CLPU was dissolved in 5 mL of dichloromethane and the solution was transferred into a homemade Teflon caster. The caster was then dried in an oven at 50 °C to remove the solvent. Films with a uniform thickness of *ca.* 0.7 mm were harvested.

3.4. General characterization and measurements

2 or CLPU was dissolved in DMF with an overall volume of 3 mL and UV-vis absorbance was then measured by using a Shimadzu UV 2550 spectrophotometer. DSC was performed on a DSC 240 F1 at a heating rate of 10 °C min^{-1} under a N_2 atmosphere. The heat flow between 0 to 120 °C was recorded. Variable temperature XRD measurements were conducted on a Bruker D8 Discover diffractometer (λ = 0.154 nm). NIR (λ = 807 nm) irradiation was generated by using a STL808T1-15W fibre-coupled laser system (Stone Company) and the local temperature as a function of time was recorded by using an FLIR A35 FOV 24 thermal imaging camera. For thermogravimetric analysis (TGA) tests, samples of about 8.0 mg were loaded onto a TA STD Q600 instrument under a nitrogen atmosphere and the weight loss was monitored from 40 to 800 °C at a heating rate of 10 °C min^{-1}.

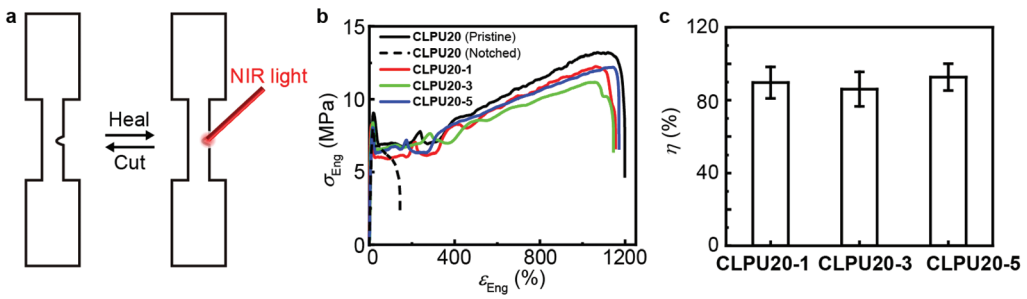

Fig. 6 Recovery of the mechanical properties of **CLPU20** films after healing. (a) Dog-bone shaped specimens with a notch (0.5 mm wide) at a gauge section (gauge width 2.0 mm). (b) Typical stress–strain curves of pristine, notched, and healed specimens. (c) Healing efficiency, η, after multiple notching–healing cycles.

3.5. Small angle X-ray scattering (SAXS)

SAXS tests were performed on an Anton-Paar SAXess mc^2 platform using slit collimation (slit dimensions: 20 × 0.33 mm^2). The camera length was 260 mm and the exposure time was 5 minutes. The 1D scattering intensity was desmeared automatically using the commercial software SAXSqudrant and plotted as a function the magnitude of the scattering vector $q = 4\pi/\lambda \sin(\theta)$, where λ is the wavelength of the X-ray (0.154 nm) and 2θ is the scattering angle.

3.6. Mechanical tests

The mechanical properties of CLPU films were determined on an Instron 3343 machine. Dog-bone shaped specimens were punched from films with a cutter. The width and the length of the gauge section were 2 mm and 5 mm, respectively. Small pieces of the same material were wrapped around the testing specimen in the regions of the clamps to minimize slippage. Specimens were stretched at a cross-head speed of 0.25 mm s^{-1} and the data were interpreted in terms of engineering stress $\sigma_{Eng} = F/S_0$ (F is the force at the grips and S_0 is the area of the cross-section of the as-prepared specimen) as a function of engineering strain $\varepsilon_{Eng} = (l - l_0)/l_0 \times 100\%$ (l_0 and l are the distance between the grips before and after stretching).

Cracks (0.5 mm deep) were cut on the sample surface by using a razor blade and irradiated by NIR light for a given time. Images of cracks before and after healing were recorded with an optical microscope (XDS-1, Guangzhou Liss Optical Instrument Co., Ltd). To evaluate the healing of mechanical properties, a 0.5 mm wide notch was made at the gauge section of dog-bone shaped specimens and irradiated with NIR light for a prescribed time. For some specimens, the cutting and healing procedures were repeated several times. The mechanical properties of the specimens were determined and the healing efficiency η is defined as the ratio of material toughness (the area under stress–strain curves) of the healed specimen to that of the pristine one.

4. Conclusions

In summary, we present in this study a series of novel carbolong polyurethanes that are capable of fast, spatially resolved, and repeated self-healing under NIR light irradiation in a remote and programmable way. The covalently linked carbolong complex endows the metallopolymers with excellent photothermal properties that depend on the content of carbolong complexes and the power density of NIR irradiation. The capacity of light-to-heat conversion allows these metallopolymers with a very low carbolong content to heal efficiently and the healing process can be spatially controlled with high precision by a laser pattern. This work represents the first example where the healing of metallopolymers is triggered by the NIR photothermal effect of the organometallic complex. Although in our first demonstration we focused on polyurethanes with simple non-covalent interactions (*i.e.*, polymer crystallization and hydrogen bonding), we envisage that carbolong complexes are versatile and will be applicable to a wide range of more advanced polymers of various forms such as fibres, elastomers, composites and so on. We are currently broadening the uses of carbolong complexes by integrating them with thermo-reversible motifs other than simple hydrogen bonding and polymer crystallites, such as strong multiple hydrogen bonding, dynamic covalent adducts, liquid crystalline components, *etc.*, into polymers of various chemical structures and hierarchical topologies, targeting a wider variety of light programmable materials and light-powered actuators.

Conflicts of interest

The authors declare no competing financial interest.

Acknowledgements

This work was financially supported by the National Natural Science Foundation of China (No. 21472155, 21490573, and U1705254).

References

1 G. R. Whittell, M. D. Hager, U. S. Schubert and I. Manners, *Nat. Mater.*, 2011, **10**, 176–188.
2 R. A. Musgrave, A. D. Russell, D. W. Hayward, G. R. Whittell, P. G. Lawrence, P. J. Gates, J. C. Green and I. Manners, *Nat. Chem.*, 2017, **9**, 743.
3 M. Burnworth, L. Tang, J. R. Kumpfer, A. J. Duncan, F. L. Beyer, G. L. Fiore, S. J. Rowan and C. Weder, *Nature*, 2011, **472**, 334–338.
4 R. Shunmugam and G. N. Tew, *J. Am. Chem. Soc.*, 2005, **127**, 13567–13572.
5 Q. Dong, G. Li, C.-L. Ho, C.-W. Leung, P. W.-T. Pong, I. Manners and W.-Y. Wong, *Adv. Funct. Mater.*, 2014, **24**, 857–862.
6 D. Astruc, E. Boisselier and C. Ornelas, *Chem. Rev.*, 2010, **110**, 1857–1959.
7 S. Liu, K. Zhang, J. Lu, J. Zhang, H.-L. Yip, F. Huang and Y. Cao, *J. Am. Chem. Soc.*, 2013, **135**, 15326–15329.
8 T.-L. Choi, K.-H. Lee, W.-J. Joo, S. Lee, T.-W. Lee and M. Y. Chae, *J. Am. Chem. Soc.*, 2007, **129**, 9842–9843.
9 S. Han, Y. Feng, F. Zhang, C. Yang, Z. Yao, W. Zhao, F. Qiu, L. Yang, Y. Yao, X. Zhuang and X. Feng, *Adv. Funct. Mater.*, 2015, **25**, 3899–3906.
10 S. Bode, M. Enke, R. K. Bose, F. H. Schacher, S. J. Garcia, S. van der Zwaag, M. D. Hager and U. S. Schubert, *J. Mater. Chem. A*, 2015, **3**, 22145–22153.
11 S. Nagappan, S. S. Park, E. J. Yu, H. J. Cho, J. J. Park, W.-K. Lee and C.-S. Ha, *J. Mater. Chem. A*, 2013, **1**, 12144–12153.
12 J. Yuan, X. Fang, L. Zhang, G. Hong, Y. Lin, Q. Zheng, Y. Xu, Y. Ruan, W. Weng, H. Xia and G. Chen, *J. Mater. Chem.*, 2012, **22**, 11515–11522.

13 G. Hong, H. Zhang, Y. Lin, Y. Chen, Y. Xu, W. Weng and H. Xia, *Macromolecules*, 2013, **46**, 8649–8656.
14 W. Weng, X. Fang, H. Zhang, H. Peng, Y. Lin and Y. Chen, *Eur. Polym. J.*, 2013, **49**, 4062–4071.
15 J. Yuan, H. Zhang, G. Hong, Y. Chen, G. Chen, Y. Xu and W. Weng, *J. Mater. Chem. B*, 2013, **1**, 4809–4818.
16 B. Yang, H. Zhang, H. Peng, Y. Xu, B. Wu, W. Weng and L. Li, *Polym. Chem.*, 2014, **5**, 1945–1953.
17 J. C. Li, H. Ejima and N. Yoshie, *ACS Appl. Mater. Interfaces*, 2016, **8**, 19047–19053.
18 Z. Lu, Y. Cai, Y. Wei, Q. Lin, J. Chen, X. He, S. Li, W. Wu and H. Xia, *Polym. Chem.*, 2018, **9**, 2092–2100.
19 X. He, X. He, S. Li, K. Zhuo, W. Qin, S. Dong, J. Chen, L. Ren, G. Liu and H. Xia, *Polym. Chem.*, 2017, **8**, 3674–3678.
20 Z. Lu, Q. Lin, Y. Cai, S. Chen, J. Chen, W. Wu, X. He and H. Xia, *ACS Macro Lett.*, 2018, **7**, 1034–1038.
21 C. Zhu, M. Luo, Q. Zhu, J. Zhu, P. V. Schleyer, J. I. Wu, X. Lu and H. Xia, *Nat. Commun.*, 2014, **5**, 3265.
22 C. Zhu, C. Yang, Y. Wang, G. Lin, Y. Yang, X. Wang, J. Zhu, X. Chen, X. Lu, G. Liu and H. Xia, *Sci. Adv.*, 2016, **2**, e1601031.
23 Q. Zhuo, J. Lin, Y. Hua, X. Zhou, Y. Shao, S. Chen, Z. Chen, J. Zhu, H. Zhang and H. Xia, *Nat. Commun.*, 2017, **8**, 1912.
24 C. Zhu and H. Xia, *Acc. Chem. Res.*, 2018, **51**, 1691–1700.
25 C. Zhu, S. Li, M. Luo, X. Zhou, Y. Niu, M. Lin, J. Zhu, Z. Cao, X. Lu, T. Wen, Z. Xie, P. v. R. Schleyer and H. Xia, *Nat. Chem.*, 2013, **5**, 698.
26 C. Zhu, Y. Yang, J. Wu, M. Luo, J. Fan, J. Zhu and H. Xia, *Angew. Chem., Int. Ed.*, 2015, **54**, 7189–7192.
27 R. Li, Z. Lu, Y. Cai, F. Jiang, C. Tang, Z. Chen, J. Zheng, J. Pi, R. Zhang, J. Liu, Z.-B. Chen, Y. Yang, J. Shi, W. Hong and H. Xia, *J. Am. Chem. Soc.*, 2017, **139**, 14344–14347.
28 C. Zhu, Y. Yang, M. Luo, C. Yang, J. Wu, L. Chen, G. Liu, T. Wen, J. Zhu and H. Xia, *Angew. Chem., Int. Ed.*, 2015, **54**, 6181–6185.
29 Q. Lin, S. Li, J. Lin, M. Chen, Z. Lu, C. Tang, Z. Chen, X. He, J. Chen and H. Xia, *Chem. – Eur. J.*, 2018, **24**, 8375–8381.
30 D. Habault, H. Zhang and Y. Zhao, *Chem. Soc. Rev.*, 2013, **42**, 7244–7256.
31 Y. Li, S. Chen, M. Wu and J. Sun, *ACS Appl. Mater. Interfaces*, 2014, **6**, 16409–16415.
32 H. Zhang and Y. Zhao, *ACS Appl. Mater. Interfaces*, 2013, **5**, 13069–13075.
33 X. Yin, Y. Zhang, P. Lin, Y. Liu, Z. Wang, B. Yu, F. Zhou and Q. Xue, *J. Mater. Chem. A*, 2017, **5**, 1221–1232.
34 Y. Liu, X. Pei, Z. Liu, B. Yu, P. Yan and F. Zhou, *J. Mater. Chem. A*, 2015, **3**, 17074–17079.
35 N. Manuel, M. Rémi, Z. Baolei, B. Alejandro, H. Sebastian, B. Fabian, S. Sebastian, M. Rolf and W. Andreas, *Adv. Funct. Mater.*, 2017, **27**, 1700767.
36 Q.-T. Li, M.-J. Jiang, G. Wu, L. Chen, S.-C. Chen, Y.-X. Cao and Y.-Z. Wang, *ACS Appl. Mater. Interfaces*, 2017, **9**, 20797–20807.
37 F. I. Altuna, J. Antonacci, G. F. Arenas, V. Pettarin, C. E. Hoppe and R. J. J. Williams, *Mater. Res. Express*, 2016, **3**, 045003.
38 P. Peng, B. Zhang, Z. Cao, L. Hao, F. Yang, W. Jiao, W. Liu and R. Wang, *Compos. Sci. Technol.*, 2016, **133**, 165–172.
39 X.-Q. Xu, Z. Wang, R. Li, Y. He and Y. Wang, *Chem. – Eur. J.*, 2018, **24**, 9769–9772.
40 L. Yang, X. Lu, Z. Wang and H. Xia, *Polym. Chem.*, 2018, **9**, 2166–2172.
41 Y. I-Kuan and L. C. Yun, *J. Polym. Sci., Part B: Polym. Phys.*, 2010, **48**, 1777–1785.
42 T. Kamal, T. J. Shin and S.-Y. Park, *Macromolecules*, 2012, **45**, 8752–8759.
43 N. Stribeck, in *X-Ray Scattering of Soft Matter*, ed. H. Pasch, Springer, 2007, ch. 8, pp. 117–118.
44 C. L. Lewis, Y. Meng and M. Anthamatten, *Macromolecules*, 2015, **48**, 4918–4926.
45 C. Huang, M. Jevric, A. Borges, S. T. Olsen, J. M. Hamill, J.-T. Zheng, Y. Yang, A. Rudnev, M. Baghernejad, P. Broekmann, A. U. Petersen, T. Wandlowski, K. V. Mikkelsen, G. C. Solomon, M. Brøndsted Nielsen and W. Hong, *Nat. Commun.*, 2017, **8**, 15436.

